Thermal separation in near-axis boundary layers with intense swirl

M. A. Herrada, M. Pérez-Saborid, and A. Barrero
Escuela Superior de Ingenieros, Universidad de Sevilla, 41092 Sevilla, Spain

Swirling flows have a wide range of applications and exhibit a variety of interesting features. Gas cooling near the axis in these flows, the so-called Ranque–Hilsch effect, is one of them. To gain insight into this phenomenon, we have analyzed the thermal, near-axis boundary layer of a gas jet driven by a class of conical inviscid quasi-incompressible flows whose axial and azimuthal velocity components, w and v, and stagnation temperature, T_t, behave near the axis as $w = W_0 r^{m-2}$, $v = L W_0 r^{m-2}$, and $T_t - T_r = T_0 r^{2(m-2)}$, where z and r are the axial and radial coordinates, L is the Squire number directly related to the swirl strength, m is any real number such as $1 \leq m < 2$, T_r is a reference temperature, and W_0 and T_0 are arbitrary dimensional constants; W_0 is assumed to be positive while T_0 may be either positive or negative. To simplify the boundary layer analysis, low Mach number flows with small relative variations in the gas density have been considered. Radial profiles of axial and azimuthal velocity components, and static and stagnation temperatures are found to depend on the Squire parameter L, the Prandtl number, Pr, and the rest of the parameters of the problem. Even for the case of inviscid vortices with positive values of T_0, for which the stagnation temperature increases towards the axis, is found that the stagnation temperature decreases substantially in the vortex core for some range of values of both L and Pr (Ranque–Hilsch effect) when the effect of both heat conduction and the work done by viscous forces are taken into account. It is also found that there exists an optimum value L_{op} for which the cooling effect reaches a sharp maximum and that small deviations of L from L_{op} reduce drastically the cooling effect. The appropriate tuning of L_{op} can be dramatically important for the efficient operation of Ranque–Hilsch tubes. The influence of the Prandtl number and the rest of the parameters of the problem has been also considered. © *1999 American Institute of Physics.* [S1070-6631(99)02111-X]

I. INTRODUCTION

Thermal energy separation often presents itself in swirling gas jets at high Reynolds numbers. In these cases, substantial variations of the stagnation gas temperature along the radial distance to the axis are observed. The colder gas flows near the axis while the hotter one is located at its periphery. This phenomenon must be added to the list of interesting and striking features exhibited by swirling flows (vortex breakdown, hysteresis, collapse of solutions, etc.). The effect of thermal separation was first reported by George Ranque[1] in 1933, and the first detailed study of this problem was published by Rudolf Hilsch[2] in 1940. Since then, numerous papers, technical reports, and patents have explored the capabilities of devices based on this effect to be used as low cost, environmentally clean, refrigerators. A list of relevant papers on the subject can be found in Refs. 3 and 4.

Although Ranque–Hilsch vortex tubes are commercially available, their use is limited because their efficiency is low compared to that of conventional air conditioners. Successful attempts to improve the efficiency of these devices require a deeper knowledge of the thermal separation effect. A few competing explanations of thermal separation have been given in the past. Some of them emphasize the role of turbulent heat transport in thermal separation (see Refs. 5 and 6 among others). Kurosaka[7] investigated the role of nonsteady effects (acoustic effects) as being responsible for thermal

separation. In his experiment, Kurosaka found that effective thermal separation is usually accompanied by a loud whistle. Nonetheless, neither acoustic effects nor turbulent transport mechanisms seem to be essential for thermal separation. In effect, turbulence should tend to eliminate nonhomogeneities in the flow rather than to create them, and loud whistles are seldom emitted by commercial Ranque tubes. Only much shorter tubes, like those used in Kurosaka's experiment, emit such a loud whistle.

The use of simple mathematical solutions of the Navier–Stokes equations to model thermal effects in a vortex core was first carried out by Rott,[8] who used a circulatory motion of the Burger's type superposed to an axisymmetric stagnation point meridional flow. More recently, the possibility of using conical solutions of the Navier–Stokes equations to model some basic aspects of the flow inside vortex tubes has been pointed out in Ref. 9. In any case, the lack of a self-consistent, physically realistic, mathematical model of thermal separation puts severe obstacles to improving the efficiency of vortex tubes.

The flow inside Ranque–Hilsch is quite complicated. Basically, it consists of compressed air which enters the tube with a strong swirling velocity component. The flow is focused toward a stagnation point P by means of a control valve at the tube exit, see Fig. 1. The dividing stream surface D separates the hot gas stream which leaves the tube through

3678

Phys. Fluids, Vol. 11, No. 12, December 1999

Thermal separation in near-axis boundary layers . . .   3679
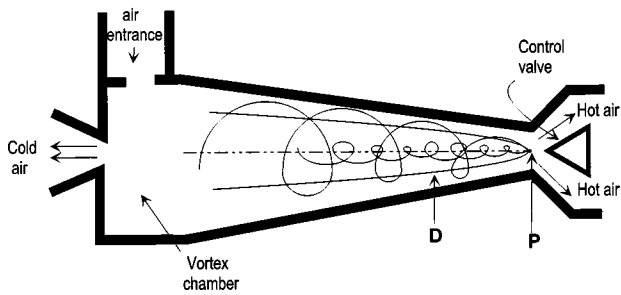
FIG. 1. The flow inside a vortex tube.

FIG. 2. The considered class of conical inviscid and nonconducting flows.

the control valve from the cold air which is forced to move back along the tube axis toward the opposite end. This helical counter flow is essential to generate the high swirling velocities near the axis needed to decrease the pressure and achieve an efficient expansion and cooling of the air.

The Reynolds number of the flow inside Ranque tubes and other vortex devices is very large, so that, viscous and conduction effects are restricted to thin boundary layers near the axis and tube walls. In the incompressible case, valuable information for the understanding of swirling flows and some of the interesting phenomena they exhibit (vortex breakdown, etc.) have been obtained from the analysis of some simplified, self-similar, near-axis boundary layers.[10,11] Reference 11 contains the analysis of the incompressible boundary layer driven by a class of inviscid vortical motion[12] which satisfies Euler equations and whose axial and azimuthal velocities, w and v, and pressure behave near the axis in the form

$$w = W_0 r^{m-2}, \tag{1}$$

$$v = \pm L W_0 r^{m-2}, \tag{2}$$

$$\frac{p}{\rho} = \frac{p_r}{\rho} + \frac{(LW_0)^2}{2(m-2)} r^{2(m-2)}, \tag{3}$$

where r is the distance to the axis and $1 \leq m < 2$. In Eqs. (1)–(3) p_r is a reference pressure and ρ is the fluid density. W_0 and L are arbitrary (positive) constants. The swirl, or Squire, parameter L is given by

$$L \equiv \|v/w\|_{r \to 0}, \tag{4}$$

and represents the ratio between azimuthal and axial inviscid velocities near the axis.

Although the flow field variables given by Eqs. (1)–(3) have cylindrical symmetry, they correspond to the near-axis behavior ($r/z \ll 1$) of a family of conically similar solutions to the incompressible Euler equations resulting from the superposition of a meridional flow like the one sketched in Fig. 2 plus an azimuthal motion.

The case $m = 1$, which has been broadly considered, corresponds to Long's vortex.[10] The viscous vortex cores for $m \neq 1$ analyzed in Ref. 11 are also of interest since, as suggested by many experimental data, the azimuthal velocity of the inviscid flow around real vortex cores is not exactly irrotational ($m = 1$) but of the form r^{-n} with the power n, in general, smaller than one (m larger than one). Therefore, the case $m \neq 1$ flows exhibit a number of features in common
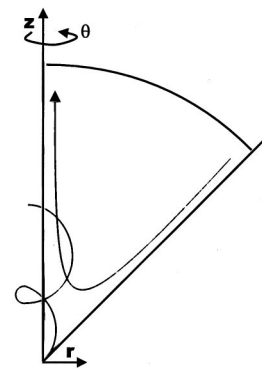
with earlier numerical and experimental results for less idealized vortices. For $m > 1$, it was shown that no boundary layer solutions exist for values of L larger than a critical one $L^*(m)$;[11] that is, no slender viscous swirling jets driven by an inviscid outer flow of the forms (1)–(3) can exist if $L > L^*$. This catastrophic behavior due to the failure of the quasi-cylindrical approximation of the boundary layer equations was interpreted as vortex breakdown. It should be pointed out that for the case $m = 1$, the outer flow and near-axis boundary layer match only for a particular value of L, $L = \sqrt{2}$.[10,11] In this case, the azimuthal and meridional motions are coupled and the parameter L is no longer suitable for the description of the $m = 1$ flows. Instead of L, Long[10] used the total axial momentum flux (flow force) to describe the viscous vortex core for the case $m = 1$. An alternative parameter S for the description of these flows, much more meaningful from the vortex breakdown point of view than the flow force, is the ratio of the maximum values of both the azimuthal and axial velocities.[13] As shown later, this parameter can be also used to describe flows with $m \neq 1$.

The results for the incompressible case, given in Ref. 11, can be used to analyze thermal boundary layers in situations where compressibility effects are relatively small. As is well known, compressibility effects can be neglected in the case of gas flows where both the Mach number, M, and the relative gas temperature variations, $\Delta T/T$, are small. As long as those requirements are satisfied, the mechanical and thermal problems decouple and the flow field found in Ref. 11 can be used to determine the temperature field by solving the energy equation. Thermal boundary layer approximation of such a simplified near-axis flow may provide a self-consistent, physically meaningful, and mathematically simple model for a complete parametric description of some essential features of the thermal separation effect.

Therefore, with the aim of enhancing the understanding of thermal separation in swirling flows we shall consider in this paper the simplified problem of the flow in a quasi-incompressible, thermal, near-axis boundary layer driven by the outer velocity and pressure fields (1)–(3) together with an outer temperature field which satisfies the energy equation for a quasi-incompressible, inviscid, and nonconducting fluid, and behaves near the axis as

$$T = T_r + \alpha \frac{(LW_0)^2}{2c_p(m-2)} r^{2(m-2)}, \tag{5}$$

where T_r is a reference temperature, c_p is the specific heat ratio at constant pressure, and

$$\alpha = \frac{(m-2)}{L^2} \left[\frac{2H_0 m^{(2m-4)/m}}{W_0^{4/m}} - (1+L^2) \right], \tag{6}$$

is a dimensionless parameter which contains the arbitrary dimensional constant H_0 characterizing the value of the total energy along a streamline. Equation (5) follows from the fact that the stagnation temperature

$$c_p T_t = c_p T + \frac{w^2}{2} + \frac{v^2}{2} = c_p T_r + H(\Psi), \tag{7}$$

remains constant along the streamlines defined by $\Psi = $ constant. For the self-similar flows considered here, we have

$$H(\Psi) = H_0 \Psi^{(2m-4)/m} = c_p T_0 r^{2(m-2)}, \tag{8}$$

which together the flow velocity components (1) and (2) lead to Eq. (5). Note that, in addition to exponent m, the inviscid motions considered here are, therefore, characterized by three given values of the three integral constants of the inviscid motion W_0, L, and H_0 (or α) (Bernouilli, Kelvin, and stagnation enthalpy conservation theorems). Note also that for positive values of parameter α, the temperature of the gas in the inviscid motion decreases toward the axis for values of m between the interval $(0,2)$ while the stagnation temperature

$$T + \frac{w^2 + v^2}{2c_p} = T_r + \left[1 + L^2 + \frac{\alpha L^2}{m-2} \right] \frac{W_0^2}{2c_p} r^{2(m-2)}$$

$$= T_0 r^{2(m-2)}, \tag{9}$$

increases towards the axis if

$$\alpha \leq (2-m)(1+1/L^2), \quad \text{or equivalently} \quad H_0 \geq 0. \tag{10}$$

Observe that thermal separation cannot take place in steady, nonconducting, inviscid swirling (or nonswirling) flows since the total enthalpy of a fluid particle remains constant when it moves along a streamline. As we shall see in the following, the situation is quite different in the near-axis vortex core where heat conduction and the work done by viscous stresses can substantially decrease (or increase) the total enthalpy on some streamlines at the expense of increasing (decreasing) it on others.

The paper is organized as follows. The equations governing the near-axis flow with boundary conditions (1)–(3) and (5) and the resulting self-similar problems are given in Sec. II. A description of the numerical integration procedure is given in Sec. III. Section IV contains numerical results of the thermal boundary layer with a discussion of the influence of the swirl and energy parameters, L and α, on the thermal separation effect. The influence of the Prandtl number is also considered; asymptotic analyses for small and large values of the Prandtl number are also included. Finally, the results are summarized in Sec. V.

II. NEAR-AXIS BOUNDARY LAYER EQUATIONS

In a gas flow, compressibility effects can be neglected if both the relative variations of temperature $\Delta T/T$ and the Mach number M are small. Then, assuming that $\Delta T/T \ll 1$ and $M \ll 1$, the quasi-incompressible, steady, axisymmetric, near-axis boundary layer equations written in cylindrical coordinates (r, θ, z) are

$$\frac{1}{r} \frac{\partial}{\partial r}(ru) + \frac{\partial w}{\partial z} = 0, \tag{11}$$

$$\frac{v^2}{r} = \frac{\partial(p/\rho)}{\partial r}, \tag{12}$$

$$u \frac{\partial v}{\partial r} + w \frac{\partial v}{\partial z} + \frac{vu}{r} = \nu \left[\frac{1}{r} \frac{\partial}{\partial r} \left(r \frac{\partial v}{\partial r} \right) - \frac{v}{r^2} \right], \tag{13}$$

$$u \frac{\partial w}{\partial r} + w \frac{\partial w}{\partial z} = -\frac{\partial(p/\rho)}{\partial z} + \nu \left[\frac{1}{r} \frac{\partial}{\partial r} \left(r \frac{\partial w}{\partial r} \right) \right], \tag{14}$$

$$u \frac{\partial h}{\partial r} + w \frac{\partial h}{\partial z} = u \frac{\partial(p/\rho)}{\partial r} + w \frac{(\partial p/\rho)}{\partial z} + \frac{\lambda}{\rho} \left[\frac{1}{r} \frac{\partial}{\partial r} \left(r \frac{\partial T}{\partial r} \right) \right]$$

$$+ \nu \left[\left(\frac{\partial w}{\partial r} \right)^2 + \left(\frac{\partial v}{\partial r} - \frac{v}{r} \right)^2 \right], \tag{15}$$

where (u, v, w) are the components of the velocity field and $h = c_p T$ is the enthalpy of the gas; c_p, ν, and λ which are assumed constant throughout the analysis are the specific heat ratio at constant pressure, kinematic viscosity, and thermal conductivity of the fluid, respectively. Although in Ranque tubes the Mach number can be of order unity in some zones of the flow, especially at the entrance zone, it is plausible to assume that, due to the action of viscosity, the Mach number of the flow is less than unity in the neighborhood of the axis. On the other hand, typical temperature differences as those found in Ranque tubes (50 K) allow for the hypothesis $\Delta T/T \ll 1$.

Note that the mechanical problem defined by Eqs. (11)–(14) with boundary conditions (1)–(3) and the thermal problem defined by Eq. (15) and condition (5) are uncoupled and can be solved separately. The mechanical problem for the case $m = 1$ was solved by Long[10] and the more general case $0 < m < 2$ has been recently considered by Fernández-Feria et al.[11] These authors took advantage of the self-similar structure of the problem to arrive at a much more simplified problem of ordinary differential equations. Here we shall extend the analysis in a straightforward way to include thermal effects.

Defining the meridional stream function Ψ, azimuthal velocity, and pressure and temperature fields in the form

$$\Psi = \nu z f(\eta), \quad w = \Psi_r/r, \tag{16}$$

$$u = -\Psi_z/r, \quad v = \frac{\nu z}{\delta^2} \gamma(\eta),$$

$$\frac{p}{\rho} - \frac{p_r}{\rho} = \frac{(\nu z)^2}{\delta^4} \beta(\eta), \quad T - T_r = \frac{(\nu z)^2}{c_p \delta^4} \Theta(\eta), \tag{17}$$

and the boundary layer variable η

Phys. Fluids, Vol. 11, No. 12, December 1999

Thermal separation in near-axis boundary layers . . .   3681

$$\eta = r/\delta(z), \tag{18}$$

where $\delta(z)$ is the boundary layer thickness, and introducing the new variables into the boundary layer equations, one arrives at the following system if $\xi = \eta^2$ instead of η is used as independent variable:

$$\gamma^2 = 2\xi\beta', \tag{19}$$

$$2\frac{m-1}{m}\gamma f' - 2f\gamma' - \frac{f\gamma}{\xi} = 4\frac{d}{d\xi}(\xi\gamma') - \frac{\gamma^2}{\xi}, \tag{20}$$

$$\frac{2-m}{m}f'^2 + ff'' + \frac{1}{2m}[(2-m)\beta + \xi\beta'] = -2\frac{d}{d\xi}(\xi f''), \tag{21}$$

$$-2f[\Theta' - \beta'] + 4\frac{(m-2)}{m}f'[\Theta - \beta] - 16f''^2\xi$$

$$-\frac{(2\gamma'\xi - \gamma)^2}{\xi} = \frac{4}{\mathrm{Pr}}\frac{d}{d\xi}(\xi\Theta'), \tag{22}$$

where $\mathrm{Pr} = \rho\nu c_p/\lambda$ is the Prandtl number.

As shown by Eq. (1), the behavior of the meridional stream function far from the axis ($\eta\to\infty$, $\xi\to\infty$, $r\to\infty$) is

$$\Psi \to (W_0/m)r^m = (W_0/m)\delta^m\eta^m = (W_0/m)\delta^m\xi^{m/2}. \tag{23}$$

The boundary layer thickness $\delta(z)$ and the behavior at the infinity of the stream function f are given by matching Eqs. (16) and (23). Hence

$$\delta(z) = (m\nu z/W_0)^{1/m} \tag{24}$$

and

$$f \to \xi^{m/2} \quad \text{as} \quad \xi\to\infty. \tag{25}$$

The behavior at the infinity of the other dimensionless variables γ, β, and Θ are obtained by matching Eqs. (16) and (17) to Eqs. (2), (3), and (5). Then, one arrives at

$$\gamma \to mL\xi^{(m-2)/2}, \quad \beta \to \frac{(mL)^2}{2(m-2)}\xi^{m-2},$$

$$\frac{\Theta}{\beta} \to \alpha, \quad \xi\to\infty. \tag{26}$$

On the other hand, the stream function and swirling velocity must vanish at the axis, where the axial velocity, pressure, and temperature must satisfy appropriate regularity conditions. Therefore, from Eqs. (16) and (17), one has

$$f(0) = \gamma(0) = 0, \quad f'(0), \beta'(0), \Theta'(0) < \infty. \tag{27}$$

III. NUMERICAL INTEGRATION FROM THE AXIS

Although the mechanical and thermal problems are uncoupled and, therefore, they can be solved separately, it is more convenient to solve them together numerically. We have followed a numerical integration procedure entirely similar to the one carried out in Ref. 11 for the mechanical problem.

Solutions of the dimensionless equations [Eqs. (19)–(22)] behave near the axis as

$$f = f_1\xi + f_2\xi^2 + f_3\xi^3 + \cdots, \tag{28}$$

$$\gamma = \xi^{1/2}(g_0 + g_1\xi + g_2\xi^2 + \cdots), \tag{29}$$

$$\beta = \beta_0 + \beta_1\xi + \beta_2\xi^2 + \cdots, \tag{30}$$

$$\Theta = \Theta_0 + \Theta_1\xi + \Theta_2\xi^2 + \cdots. \tag{31}$$

Introducing Eqs. (28)–(31) into Eqs. (19)–(22), one determines completely all the coefficients f_i, g_i, β_i, and Θ_i in terms of the first four constants of the expansion f_1, g_0, β_0, and Θ_0. For the lower-order terms one finds

$$\beta_1 = g_0^2/2, \quad \beta_2 = g_0 g_1/2, \tag{32}$$

$$f_2 = \frac{m-2}{4m}\left(f_1^2 + \frac{\beta_0}{2}\right),$$

$$f_3 = \frac{1}{48m}[4(m-4)f_1 f_2 - (3-m)\beta_1], \tag{33}$$

$$g_1 = -g_0 f_1/(4m), \tag{34}$$

$$\Theta_1 = \mathrm{Pr}\frac{(m-2)}{m}(\Theta_0 - \beta_0)f_1, \tag{35}$$

$$\Theta_2 = \frac{\mathrm{Pr}}{8}\left[(\beta_1 - \Theta_1)f_1 + 2\frac{(m-2)}{m}(f_1(\Theta_1 - \beta_1) + 2f_2(\Theta_0 - \beta_0)) - 32f_2^2\right]. \tag{36}$$

As can be seen from Eqs. (28)–(36), there are four degrees of freedom to start the integration at $\xi = 0$. Nonetheless, the computational effort can be much reduced by taking advantage that Eqs. (19)–(22) are invariant under the uniparametric transformation group

$$f \to f, \quad \xi \to C\xi, \quad \gamma \to \gamma/C,$$

$$\beta \to \beta/C^2, \quad \Theta \to \Theta/C^2. \tag{37}$$

Similarly boundary conditions at infinity, given in Eqs. (25) and (26), can be re-scaled, so that their absolute magnitude becomes irrelevant. In effect, choosing C in Eq. (37) such that $\beta_0 = -1$, the boundary conditions at both the axis and the infinity read

$$\xi\to 0, \quad f = A_1\xi + \cdots, \quad \gamma = A_2\xi^{1/2} + \cdots,$$

$$\beta = -1 + \cdots, \quad \Theta = \hat{T}_0 + \cdots; \tag{38}$$

$$\xi\to\infty, \quad f \to (C\xi)^{m/2}, \quad \gamma \to B\xi^{(m-2)/2},$$

$$\beta \to \frac{B^2}{2(m-2)}\xi^{m-2}, \quad \Theta/\beta \to \alpha, \tag{39}$$

with

$$A_1 = f_1 C, \quad A_2 = g_0 C^{(3/2)},$$

$$\hat{T}_0 = \Theta_0 C^2, \quad B = mLC^{(m/2)}.$$

For given values of m, α, and Pr, Eqs. (19)–(22) can be integrated numerically starting from $\xi \simeq 0$ with behaviors (38) once we choose arbitrary values of the three free parameters A_1, A_2, and $\hat{T}_0$. Clearly, the correct behavior at infinity will not be met except for some exceptional values of those parameters. This circumstance requires picking up a
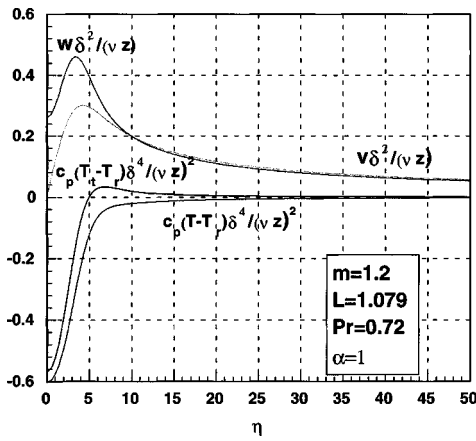
FIG. 3. Axial and azimuthal velocities and static and total temperatures as a function of the self-similar distance to the axis for $m=1.2$, $L=1.079\ 71$, $Pr=0.72$, and $\alpha=1$.

FIG. 4. Values of the right hand side of Eq. (40) as a function of the self-similar distance. It accounts for both the effect of heat conduction and the work due to viscous forces.

couple of values $A_2(A_1,m)$ and $\hat{T}_0(A_1,m,\alpha,\mathrm{Pr})$ for each real A_1 in the interval $-1/\sqrt{2}<A_1<\infty$. As shown in Ref. 11, boundary layer solutions can be characterized by the swirling parameter L which enters into the problem through the boundary conditions at infinity. It was found that there exists only one value $L(A_1)$ for each A_1 in the interval of A_1's values where boundary layer solutions exist. For $1<m<2$, $L(A_1,m)$ presents a maximum (critical) $L^*(m)$ while reaching a minimum for $0<m<1$. Therefore, for flows in the range $1<m<2$ which exhibit a number of features in common with the experimental results for less idealized vortices, there is no solution for L larger than $L^*(m)$ and there are two different solutions for each L smaller than $L^*(m)$. The occurrence of no solution of the boundary layer type for $L>L^*$ has been related to vortex breakdown.[11] The two branches in the curve $L(A_1)$ corresponding to the two possible vortices have been termed as type I $(A>A^*)$ and type II $(A<A^*)$ solutions.[14] A linear analysis of the stability of these solutions[15] shows that those of the type II are unstable for axisymmetric perturbations.

IV. NUMERICAL RESULTS

Normalized profiles of the axial and azimuthal velocity components, $\delta^2(z)w/(\nu z)$ and $\delta^2(z)v/(\nu z)$, and temperature and stagnation temperature of the gas, $c_p(T-T_r)\delta^4(z)/(\nu z)^2$ and $c_p(T_t-T_r)\delta^4(z)/(\nu z)^2$, as a function of the self-similar distance to the axis $\eta=r/\delta(z)$ have been plotted in Fig. 3 for $\mathrm{Pr}=0.72$, $\alpha=1$, $m=1.2$, and $L=1.079$. Note both the qualitative agreement of these results and those obtained from experiments in real vortex tubes[5,6] and the reduction of the stagnation temperature of the gas which takes place in the near-axis zone of the boundary layer. This phenomenon can be clarified by using the stagnation temperature equation which can be obtained by adding to Eq. (15) the result of multiplying Eqs. (13) and (14) by v and w, respectively. In self-similar variables, the stagnation temperature equation reads
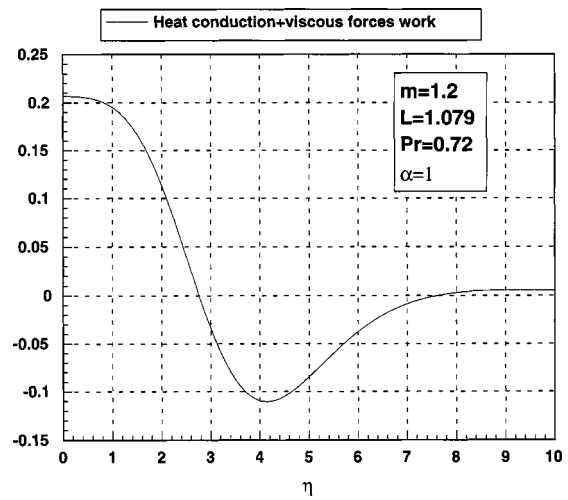
$$-2f\Theta_t' + 4\frac{m-2}{m}f'\Theta_t$$

$$= \frac{4}{\mathrm{Pr}}\frac{d}{d\xi}(\xi\Theta') + 16f''^2\xi + \frac{(2\gamma'\xi-\gamma)^2}{\xi} + 16f'\frac{d}{d\xi}(\xi f'')$$

$$+ 4\gamma\frac{d}{d\xi}(\xi\gamma') - \frac{\gamma^2}{\xi}, \tag{40}$$

where the self-similar stagnation temperature is

$$\Theta_t = \Theta + 2f'^2 + \tfrac{1}{2}\gamma^2. \tag{41}$$

Equation (40) accounts for the contribution of both thermal conduction and the work per unit volume and time done by viscous forces, and the axial and radial convective flux of total enthalpy; the right-hand side of Eq. (40) which represents the contribution of heat conduction and work by shear stresses as a function of the radial distance is plotted in Fig. 4 for the case considered in Fig. 3. As shown in Fig. 4, this contribution is positive near the axis while the radial convective flux vanishes there (the radial velocity, u, and the stream function f going to zero at the axis). Therefore, to satisfy (40), the axial convection of total enthalpy, $4(m-2)f'\Theta_t/m$, must be positive near the axis and since $m<2$, Θ_t must be necessarily negative there (stagnation temperature less than reference temperature).

In fact, the self-similar analysis shows the existence of a downstream convective flux of total enthalpy which balances the conductive heat flux toward the axis and the work of viscous forces. Therefore, as shown by expressions (41) together with (16), (17), and (24), the total enthalpy along a streamline increases downstream giving rise to a reduction of the thermal separation effect in the downstream direction. It should be pointed out that an explanation of how thermal splitting is originated cannot be provided by the self-similar analysis presented here, but it requires the study of a non-self-similar evolution of the vortex core emerging from the converging flow in the turning region close to point P in Fig. 1. For appropriate values of the parameters of the problem,
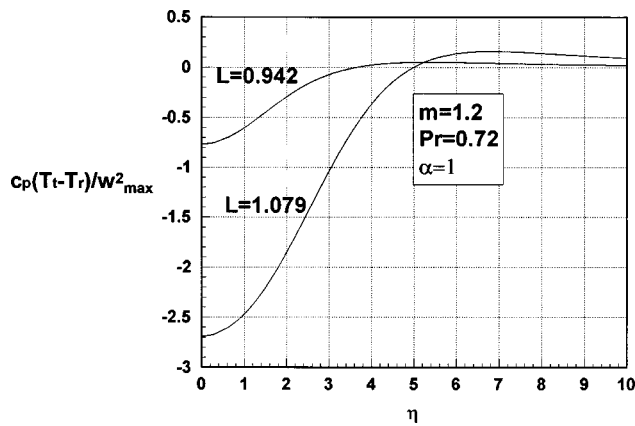
FIG. 5. Normalized stagnation temperature as a function of the self-similar distance for several values of the swirling parameter L.

FIG. 6. Normalized values of the maximum thermal separation $H = c_p(T_r - T_{t_{min}})/w_{max}^2$ as a function of L.

the structure of the viscous vortex core will evolve eventually, for sufficiently large z, to the self-similar structure presented here.

Let us discuss in the following the influence on the thermal separation phenomenon of the relevant parameters of the problem: The swirl parameter L (or the azimuthal to axial inviscid velocity ratio at the axis), the dimensionless energy constant α, the Prandtl number, and the exponent m characterizing the velocity and temperature flow field.

A. Influence of the swirl parameter L

Figure 5 shows the stagnation temperature profiles $c_p(T_t - T_r)/w_{max}^2$ for Pr$=0.72$, $\alpha=1$ and $m=1.2$ and different values of L. For convenience, the maximum value of the axial velocity have been used to normalize the stagnation temperature. Note that for a given maximum axial velocity of the swirling jet, the thermal separation effect depends strongly of the swirling parameter L.

It is useful to calculate the maximum value of the thermal separation defined as the maximum stagnation temperature jump

$$H(L) = \frac{c_p(T_r - T_{t_{min}})}{w_{max}^2}, \tag{42}$$

as a function of L. Results of $H(L)$ for $m=1.1$, Pr$=0.72$, and $\alpha=0$ are plotted in Fig. 6. The upper branch of the curve in Fig. 6 corresponds to values of A_1 larger than the critical value A_1^* while the lowest corresponds to unstable solutions of type II. The maximum value $H_{opt} = H(L_{opt})$ is reached at a certain value L_{opt} which lies very close to L^*. Note that there exists on the upper branch a very narrow interval of values of L where H is very close to the value H_{opt}. Outside this interval the cooling effect falls down abruptly. These results suggest that the efficiency of the thermal separation process in the vortices considered here critically depends on L and it may explain why devices based on the Ranque effect would not work efficiently outside a narrow range of operating conditions.

We can now investigate the validity of the quasi-incompressible flow hypothesis assumed throughout the
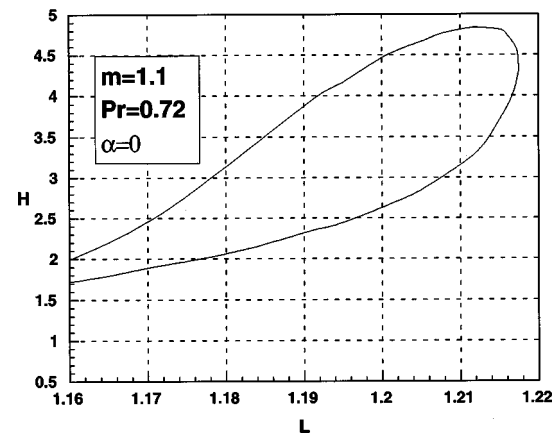
analysis; let us assume a maximum axial velocity component of the order of 100 m/s; then, using data from Fig. 6, we have that the maximum difference in the stagnation temperature is almost 50 K for values of L close to $L=1.21$ while the maximum Mach number of the flow and the maximum ratio $\Delta T/T$ are about 0.3 and $\frac{1}{6}$, respectively, which makes plausible the hypothesis of quasi-incompressible flow.

For the sake of completeness, we plot in Fig. 7 values of the maximum thermal separation for the case $m=1$, Pr $=0.72$, and $\alpha=1$. As indicated before, the relevant vortex breakdown parameter for $m=1$ is the ratio S introduced in Ref. 13 between the maximum values of the azimuthal and axial velocities but it can be also used to describe boundary layer solutions with $m \neq 1$. In fact, for a given m such as $1 \leq m < 2$ there exists two self-similar solutions if S is less than a critical value $S^*(m)$ and there are no solutions for $S > S^*$. Note that the maximum thermal separation curve versus S presents a sharp maximum. For comparison, values of the maximum thermal separation has been also plotted for the cases $m=1.1$ and $m=1.2$. Figure 7 shows that for a given value of parameter S, H reaches its minimum for a value of m between the interval $1 < m < 1.2$. Note that the
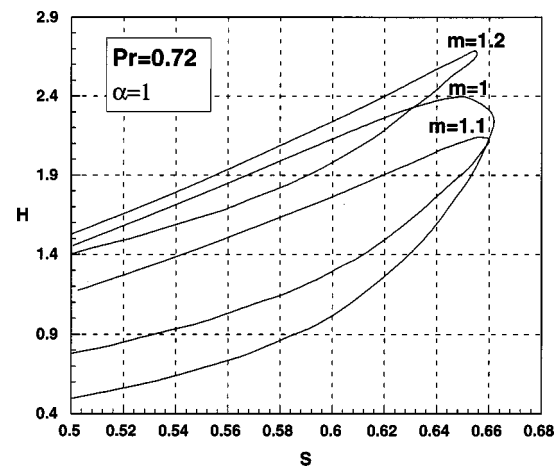
FIG. 7. Normalized values of the maximum thermal separation $H = c_p(T_r - T_{t_{min}})/w_{max}^2$ as a function of S for three different values of m.
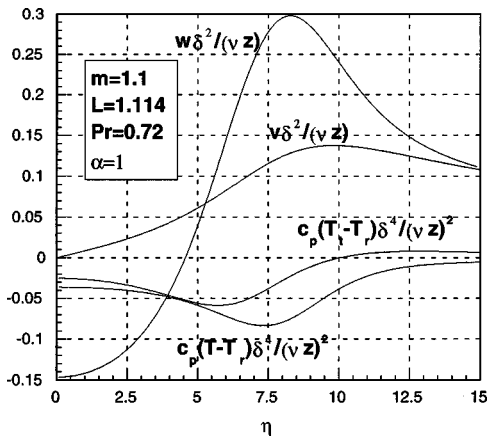
FIG. 8. Radial profiles of the axial and azimuthal velocities and static and total temperatures for a typical two cell regime.

FIG. 9. Normalized total temperature profiles for three different values of α.

value of the exponent m influences not only the matching conditions far from the axis but also the numerical values of the coefficients of the boundary layer equations.

Figure 8 shows the results obtained for a flow of the type II (unstable solutions) for the indicated values of L, α, and m in the figure. In this case, a two-cell flow develops where the fluid moves towards the origin (negative velocities) near the axis and in the opposite direction (positive velocities) away from it. Note that the minimum temperature is reached outside the axis and just near the point corresponding to the maximum values of the azimuthal and axial velocity.

B. Influence of the energy parameter α

The conservation energy equation of the class of inviscid and nonconducting gas flow we have considered for matching the conducting and viscous vortex core requires that the stagnation temperature of the gas behaves near the axis as

$$T_t = T_r + \left(1 + L^2 + \frac{\alpha L^2}{m-2}\right)\frac{W_o^2}{2c_p} r^{2m-4}. \quad (43)$$

For values of α such as $0 \le \alpha < (2-m)(1+1/L^2)$ the stagnation temperature increases toward the axis and it decreases if $(2-m)(1+1/L^2) < \alpha$. Negative values of α has not been considered since they lead to results that are quite unrealistic. In fact, for $m < 2$ and $\alpha < 0$ the static gas temperature in the inviscid vortex flow increases toward the axis [see Eq. (5)]. Note that, similar to the values of W and L which are fixed by the conservation of momentum and angular momentum in the inviscid flow, the value of α is given by the conservation of total enthalpy.

The influence of α in the thermal splitting is shown in Fig. 9 where normalized profiles of the total temperature for different values of the parameter α are plotted, ($\alpha = 0, 0.5, 1, 2,$ and 3). Note that the thermal separation phenomenon depends substantially on α and its effect increases when α decreases. The explanation of this behavior lies in the fact that the heat conduction flux towards the axis decreases with α; $\alpha = 0$ corresponds to uniform outer temperatures [see Eq. (5)]. Interestingly enough are vortices with $\alpha = 2$ and 3 for which an inverse thermal separation takes
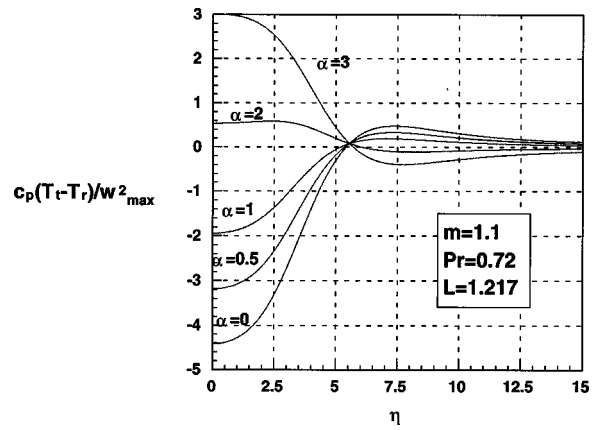
place in the viscous vortex core (increasing of the total enthalpy and heating of the gas in the near axis zone) in spite that both the static and stagnation temperatures of the inviscid vortex decrease toward the axis. In these cases, the heat conduction flux towards the axis becomes so large that both the stagnation and static temperatures increase. These results show that contrary to what one may think at first sight inviscid vortices with both static and stagnation temperatures decreasing toward the axis are not the flow structures needed to produce effective splitting thermal separation in efficient Ranque vortex tubes. The analysis given here also seems to indicate that thermal separation phenomenon is due to dissipative effects and takes place inside swirling thermal boundary layers; the influence of the high Reynolds number vortex flow on the thermal splitting is exclusively limited to the values of L and α which are external parameters for the boundary layer and they are fixed through the conservation theorems of the inviscid and nonconducting flow.

C. Influence of the Prandtl number

Figure 10 shows the dimensionless stagnation temperature profiles for three different values of the Prandtl number but identical values of the other three parameters $L = 1.113$,
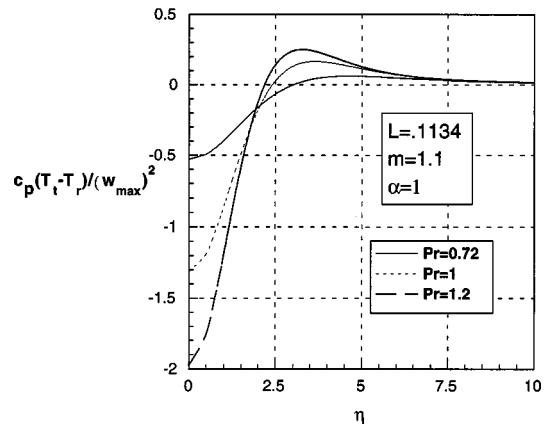
FIG. 10. Normalized total temperature profiles for three different values of the Prandtl number.

$\alpha = 1$, and $m = 1.1$. Note that both the minimum value of the stagnation temperature and the thickness of the layer where thermal separation takes place decrease with the Prandtl number.

To obtain deeper insight into both the thermal near axis boundary layer investigated here and the role that the Prandtl number plays in the thermal separation phenomenon it is of interest to analyze the boundary layer problem in the two asymptotic limit cases $Pr \to \infty$ and $Pr \to 0$, in spite of the relation $h = c_p T$ used as an equation of state which is only valid for a gas ($Pr \sim 1$).

1. Pr≫1

For large values of the Prandtl number, the thickness of the thermal boundary layer is much smaller than the viscous thickness $\delta(z)$, so that heat conduction is negligible outside the very thin inner thermal layer. In the outer viscous region, the equation governing the temperature field results of neglecting the conduction term in Eq. (22)

$$-2f[\Theta' - \beta'] + 4\frac{(m-2)}{m}f'[\Theta - \beta] - 16f''^2\xi$$

$$-\frac{(2\gamma'\xi - \gamma)^2}{\xi} = 0. \tag{44}$$

Taking into account the behaviors of the flow field variables given by Eqs. (28)–(30), it is easy to show that near the axis temperature θ behaves as

$$\Theta \to K\xi^{2(m-2)/m} \quad \text{as} \quad \xi \to 0, \tag{45}$$

where K is an unknown constant. Since temperature becomes singular near the axis, it must be regularized throughout a thermal conduction sublayer. In fact, defining the inner variables

$$s = Pr\xi, \quad \phi = \Theta Pr^{2(m-2)/m}, \tag{46}$$

Eq. (22) becomes at lowest order

$$s\frac{\partial^2\phi}{\partial s^2} + \left(1 + \frac{f_1 s}{2}\right)\frac{\partial\phi}{\partial s} - \frac{m-2}{m}f_1\phi = 0. \tag{47}$$

It may be easily verified that a solution of Eq. (47) satisfying the boundary condition at the axis behaves as

$$\phi = \phi_o\left(1 + \frac{m-2}{m}f_1 s + \cdots\right) \quad \text{as} \quad s \to 0, \tag{48}$$

where the normalized temperature ϕ_o is unknown and must be calculated from the analysis. On the other hand, at the infinity, solutions of (47) behave as

$$\phi = Js^{2(m-2)/m}, \quad \text{as} \quad s \to \infty. \tag{49}$$

The matching of behaviors (45) and (49) leads to $J = K$. Therefore, choosing an arbitrary value of ϕ_o and starting the numerical integration of Eq. (47) with behavior (48), one finds, far from the axis, the value $J(\phi_o) = K(\phi_o)$. Hence, Eq. (44) can be integrated numerically starting from $\xi \ll 1$ with condition (45) to arrive at the infinity with the behavior

$$\Theta/\beta \to \alpha^*(\phi_o), \quad \text{as} \quad \xi \to \infty, \tag{50}$$
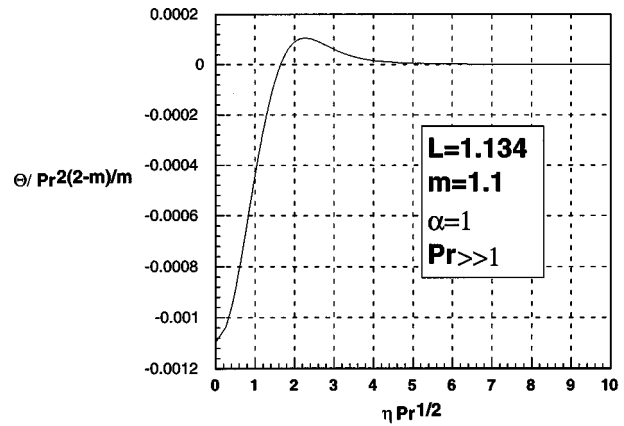
FIG. 11. Temperature profile for large values of the Prandtl number.

where β is given by Eq. (26). The value of ϕ_o which yields the correct value $\alpha^* = \alpha$ is obtained by shooting. The normalized static temperature radial profile for large values of the Prandtl number is given in Fig. 11. Note that the thickness of the layer Δ in which exists a substantial reduction of the stagnation temperature decreases with the Prandtl number, $\Delta \sim Pr^{-1/2}$ while the normalized stagnation temperature $\delta^4 c_p(T_r - T_t)/(\nu z)^2$ increases as $Pr^{2(2-m)/m}$.

2. Pr≪1

For small values of the Prandtl number the viscous layer is much thinner than the thermal boundary layer. In the viscous sublayer, temperature is uniform to lowest order, $\Theta = \Theta_0$, since heat conduction is dominant there [see Eq. (22) for values of ξ of order unity]. Introducing the new variables

$$s = \xi Pr^{2/m}, \quad \Theta = Pr^{2(2-m)/m}\phi, \tag{51}$$

into Eq. (22), one obtains to lowest order

$$s\frac{d^2\phi}{ds^2} + (1 + s^{m/2}/2)\frac{d\phi}{ds} - \frac{m-2}{2}s^{(m-2)/2}\phi = 0, \tag{52}$$

whose solution behaves near the axis as

$$\phi = \phi_o\left[1 + 2\frac{m-2}{m^2}s^{m/2} + \cdots\right], \tag{53}$$

where ϕ_o is unknown. At infinity, solutions satisfying Eq. (52) behave as

$$\phi = Ks^{m-2}, \tag{54}$$

behavior (54) together with condition (5) lead to $K = \alpha(mL)^2/[2(m-2)]$. Choosing an arbitrary value of ϕ_o (let us say ϕ_o^*) and starting the integration of Eq. (52) from the origin with behavior (53), one finds numerically at the infinity a value of K (say K^*) which in general will be different from the correct one $\alpha(mL)^2/[2(m-2)]$. Taking advantage of the linear character of Eq. (52), one can easily calculate the correct value of $\phi_o = \phi_o^*(mL)^2/[2(m-2)K^*]$.

The normalized static temperature radial profile for small values of the Prandtl number is plotted in Fig. 12. Note that the thickness Δ of the layer in which there is a substan-
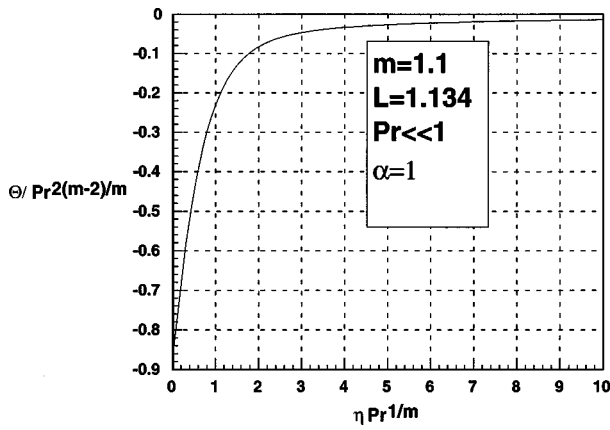
FIG. 12. Temperature profile for small values of the Prandtl number.

tial reduction of the stagnation temperature increases with the Prandtl number, $\Delta \sim \mathrm{Pr}^{2/m}$, while the normalized stagnation temperature $\delta^4 c_p (T_r - T_t)/(\nu z)^2$ decreases as $\mathrm{Pr}^{2(2-m)/m}$.

V. CONCLUSIONS

We have analyzed the quasi-incompressible thermal near-axis boundary layer flows driven by an inviscid but vortical velocity field which decays as r^{m-2} with the distance r to the axis. Far from the axis the stagnation temperature of the inviscid and nonconducting flow is

$$T_t = T_r + \left[1 + L^2 + \frac{\alpha L^2}{m-2} \right] \frac{W_0^2}{2c_p} r^{2(m-2)}, \tag{55}$$

while the static temperature is given by

$$T = T_r + \alpha \frac{(LW_0)^2}{2c_p(m-2)} r^{2(m-2)}. \tag{56}$$

The flow, which is self-similar, depends on the following parameters: The swirl parameter L (or the azimuthal to axial inviscid velocity ratio at the axis), the parameter α which characterizes the temperature field outside the thermal near-axis boundary layer, the Prandtl number, and the exponent m which characterize both the outer velocity and the temperature fields.

Profiles of velocity, temperature, and stagnation temperature as a function of the self-similar distance to the axis have been obtained for several values of the parameters as previously indicated. The obtained results agree qualitatively well with experimental measurements in the vortex tubes. Asymptotic results for large and small values of the Prandtl number have also been carried out.

As can be seen from Fig. 6, for values of m in the range of interest (slightly larger than one), the maximum value of the thermal separation in swirling axisymmetric boundary layer flows is defined as

$$H(L) = \frac{c_p (T_r - T_{t_{\min}})}{w_{\max}^2}, \tag{57}$$

and depends strongly on L. The upper branch of the curve in Fig. 6 corresponds to values of A_1 larger than the critical

value A_1 while the lowest corresponds to the unstable solutions of type II. The maximum value $H_{\mathrm{opt}} = H(L_{\mathrm{opt}})$ is reached at a certain value L_{opt} which lies very close to L^*. It is of interest to remark that a factor (almost 5) in the dimensionless temperature drops like the one shown in Fig. 6 for values of L near the optimum one accounts for the temperature measurements in Ranque–Hilsch tubes.[16] Neither acoustic effects nor turbulence are, therefore, needed to explain the occurrence of thermal separation in vortex tubes. Note also that the upper branch in Fig. 6 presents a *plateau* in a very narrow interval of values of L where H is very close to the value H_{opt}. Outside this interval the cooling efficiency falls down abruptly. These results show that the efficiency of the thermal separation process in the vortices considered here depends critically on L and suggests that devices based on the Ranque effect will not work efficiently outside a narrow range of operating conditions.

For the sake of completeness, in Fig. 7 we have plotted values of the normalized maximum cooling for the case $m = 1$. As was indicated previously, the relevant vortex breakdown parameter for $m = 1$ is the ratio between the maximum values of the azimuthal and axial velocities S introduced in Ref. 13. For a given m such $1 \leqslant m < 2$, there exists two self-similar solutions if S is less than a critical one $S^*(m)$ and there are no solutions for $S > S^*$. Note that the normalized maximum cooling curve versus S presents a sharp maximum. For comparison, values of the normalized maximum cooling has been plotted for the cases $m = 1.1$ and $m = 1.2$.

The effect of the Prandtl number on the thermal splitting has been also investigated. Asymptotic results for large and small values of the Prandtl number are given. We found that thermal separation increases with the Prandtl number; in particular the scaling for large and small values of the Prandtl number is

$$T_r - T_t \sim \mathrm{Pr}^{2(2-m)/m}, \tag{58}$$

which shows that when $\mathrm{Pr} \to 0$ the thermal splitting is negligible ($m < 2$) due to the smoothness effect of heat conduction.

The radius of the core where the gas is cooled $R(z)$ depends also on the Prandtl number. For Prandtl of order unity, this thickness is of the order of the viscous core $\delta(z)$ given by (24). For large values of the Prandtl number the radius of the thermal core is of the order of $\delta(z)/\mathrm{Pr}^{1/2} \ll \delta(z)$ while it is of the order of $\delta \mathrm{Pr}^{-1/m} \gg \delta$ for small values of Pr.

The results of the self-similar analysis allows for determining some characteristic values such as the cooled gas flow rate $G(z)$ or the mean stagnation temperature which may be useful in Ranque vortex tubes. In fact, the characteristic value of the cooled gas flow rate M can be also estimated from

$$G(z) = 2\pi \int_o^\infty w r \, dr. \tag{59}$$

As usual in boundary layer analysis, this integral is unbounded, so that the integration must be limited to distances from the origin where the axial velocity, for instance, reaches

an arbitrary fixed value (5%, 10%) of its maximum value. Taking into account Eqs. (16) and (18) one has

$$G(z) = 2\pi\nu z \int_o^\eta f' d\eta = 2\pi\nu z \eta^m, \qquad (60)$$

if Eq. (25) is used. Choosing and arbitrary value $\eta = 10$, for which is the case given in Fig. 3, is still larger than 10% of the maximum axial velocity and assuming a columnar air vortex of typical length $z = 30$ cm, one has for the data of Fig. 3 $G = 0.6 \, \ell \, \text{s}^{-1}$. This characteristic value agrees well with the typical values of the cooled flow rate in commercially available vortex tubes of the dimensions considered here.

Analogously, the mean stagnation temperature $\overline{T_t}$ of the cooled gas can be defined as

$$\overline{T_t} - T_r = \frac{2\pi}{M(z)} \int_o^\infty (T_t - T_r) w r \, dr, \qquad (61)$$

which in self-similar variables becomes

$$\overline{T_t} - T_r = \frac{(\nu z)^2}{c_p \delta^4} \frac{1}{\eta^m} \int_o^\infty \Theta_t f' d\eta. \qquad (62)$$

Using Eq. (58), it is easy to verify that the mean temperature scales up the Prandtl number as $\text{Pr}^{2(2-m)/m}$.

Let us finally discuss the validity of the self-similar temperature field given by Eq. (17). As is well known, these self-similar solutions are not valid near the origin ($z \to 0$) where the flow turns back. Viscous dissipation is important in this region and since the flow there cannot be solved analytically its effect has been modeled elsewhere by means of a heat point source at the origin.[17] The resulting temperature field is then $T - T_r = q/z$, where q is related to the total heat flux from the source. Clearly, the self-similar solution presented here will be valid as long as

$$\frac{q}{z} \ll q^* z^{2m-4}, \qquad (63)$$

where

$$q^* = \nu^{(2m-4)/m} \left(\frac{W_0/m}{c_p^{m/4}} \right)^{4/m}. \qquad (64)$$

Therefore, the self-similar solution is valid in a region defined by

$$z \ll (q^*/q)^{1/(3-2m)} \quad \text{if} \quad 1 \leq m \leq 3/2, \qquad (65)$$

or

$$z \gg (q^*/q)^{1/(3-2m)} \quad \text{if} \quad 3/2 < m < 2. \qquad (66)$$

ACKNOWLEDGMENTS

[1] G. J. Ranque, ''Experiences sur la deténte giratoire avec productions simultaneé d'air chaud et d'un échappement d'air froid,'' J. Phys. Radium **4**, 112 (1933).

[2] R. Hilsch, ''Die expansion von Gasen in zentrifugalfeld als Kaelterprocess,'' Z. Naturforsch. **1**, 203 (1946) [see also: ''The use of the expansion of gases in a centrifugal field as a cooling process,'' Rev. Sci. Instrum. **18**, 108 (1947)].

[3] A. K. Gupta, D. G. Lilley, and N. Syred, *Swirl Flows* (Abacus, Cambridge, MA, 1985).

[4] A. Ogawa, *Vortex Flows* (CRC, Boca Raton, 1992).

[5] R. G. Deissler and M. Perlmutter, ''An analysis of flow and energy separation in a turbulent vortex,'' Int. J. Heat Mass Transf. **1**, 173 (1960).

[6] H. H. Bruun, ''Experimental investigation of the energy separation in vortex tube,'' J. Fluid Mech. **11**, 551 (1969).

[7] M. Kurosaka, ''Acoustic streaming in swirling flow and the Ranque-Hilsch effect,'' J. Fluid Mech. **124**, 139 (1982).

[8] N. Rott, ''On the viscous core of a line vortex II,'' J. Appl. Math. Phys. (ZAMP) **10**, 73 (1959).

[9] V. Shtern, A. Borissov, and F. Hussain, ''Vortex sinks with axial flow: Solutions and applications,'' Phys. Fluids **9**, 2941 (1997).

[10] R. L. Long, ''A vortex in an infinite viscous fluid,'' J. Fluid Mech. **11**, 611 (1961).

[11] R. Fernández-Feria, J. Fernández de la Mora, and A. Barrero, ''Solution breakdown in a family of self-similar nearly inviscid axisymmetric vortices,'' J. Fluid Mech. **305**, 77 (1995).

[12] R. Fernández-Feria, J. Fernández de la Mora, M. Pérez-Saborid, and A. Barrero, ''Conically similar swirling flows at high Reynolds numbers,'' Quarterly J. Mech. Appl. Math. (to be published).

[13] V. Shtern and M. A. Herrada, ''Minimum pressure coefficient in swirling jets,'' (unpublished).

[14] O. R. Burggraf and M. R. Foster, ''Continuation or breakdown in tornado-like vortices,'' J. Fluid Mech. **80**, 685 (1977).

[15] R. Fernández-Feria, ''Viscous and inviscid instabilities of non-parallel self-similar axisymmetric vortex cores,'' J. Fluid Mech. **323**, 339 (1996).

[16] E. R. G. Eckert, ''Experiments on energy separation in fluid streams,'' Mech. Eng., 58 (1984).

[17] V. Shtern, A. Borissov, and F. Hussain, ''Temperature distribution in swirling jets,'' Int. J. Heat Mass Transf. (to be published).